Applied Surface Science Advances 30 (2025) 100884

Contents lists available at ScienceDirect

Applied Surface Science Advances

journal homepage: www.sciencedirect.com/journal/applied-surface-science-advances

Effect of Al doping on structural, electronic, mechanical, and optical properties of VN thin films

Amit Kumar Verma [a], Rachana Gupta [a], Pooja Gupta [b], Sanjay Rai [b], Shashi Prakash [a], Akhil Tayal [c], Andrei Gloskovskii [c], R. Ramaseshan [d], Parveen Garg [e], Uday Deshpande [e], Mukul Gupta [e,*]

[a] Applied Science Department, Institute of Engineering and Technology, DAVV, Indore, 452001, India
[b] Indus Synchrotron Utilisation Section, Raja Ramanna Centre for Advanced Technology, Indore, 452013, India
[c] Deutsches Elektronen-Synchrotron DESY, Notkestrasse 85, Hamburg, D-22607, Germany
[d] Surface and Thin Films Studies Section, SSSD, MSG, IGCAR, Kalpakkam, 603102, India
[e] UGC-DAE Consortium for Scientific Research, University Campus, Khandwa Road, Indore, 452001, India

ARTICLE INFO

Keywords:
Transition metal nitrides
Vanadium nitride
Reactive magnetron sputtering

ABSTRACT

In this work, we present a comprehensive study of Al doped VN thin films with $x = 0$, 35, 60, 71, 84, 100 % in $V_{1-x}Al_xN$. These samples were deposited using a reactive magnetron sputtering process at room temperature (300 K), keeping the partial nitrogen gas flow fixed at 25 %. The crystal structure of samples was analyzed using synchrotron-based grazing incidence x-ray diffraction (GIXRD). Without Al doping, the phase formed is fcc-VN nd Al doping upto 71 % retains the parent VN phase. However, with 84 % Al doping the structure transforms and becomes analogous to that of hcp-AlN. This implies that the homogeneity range of Al doping in VN is considerably large. The electronic structure was measured by combining x-ray absorption (XAS) hard x-ray photoelectron spectroscopy (HAXPES) measurements. XAS measurements reveal an improvement in covalent character and structural stability in $V_{1-x}Al_xN$ films. HAXPES measurements at V 2p, N 1 s and Al 2 s core levels revel that there exists finite charge transfer between atoms. The optical properties were investigated using uv-vis spectroscopy, where the optical band gaps vary between 3.4 and 5 eV. The nanoindentation measurements were performed in these samples to measure the hardness and it was found that the hardness increases with increasing Al concentration. Overall, Al doping in VN results in significant improvements in hardness. The phase formed with 71 at.% Al doping was found to be optimal with a band gap of about 3.4 eV with fcc VN structure and hardness comparable to that of AlN.

1. Introduction

Hard coatings of early transition metal nitrides (TMNs) have been widely used in surface protection for manufacturing equipment due to their outstanding mechanical and tribological properties [1,2]. In the last decades, TMN thin films, such as TiN and CrN, have been widely utilized in the cutting tool industry due to their exceptional mechanical properties and chemical stability [3,4]. However, their relatively poor wear resistance at high temperatures is a drawback that limits the application [5]. For wear-protective applications, TMNs are commonly alloyed with aluminum (Al) to improve the thermal stability and resistance to high-temperature oxidation [6,7]. The main challenge is to maintain the structure while preventing the precipitation of the thermodynamically preferred, wurtzite aluminum nitride (hcp-AlN) phase, which can degrade coating properties [8]. TiAlN [9] and CrAlN [10] are widely studied transition metal aluminum nitride (TMAlN) systems.

Vanadium nitride (VN) based coatings can be employed as high-temperature lubrication that are deposited by physical or chemical vapor deposition [11]. VN crystallizes in a cubic rocksalt (RS) structure (SG: $Fm\bar{3}m$) and exhibits interesting properties such as high hardness [12], low friction coefficient, and superconductivity [13]. On the other hand, there is a growing interest in group-III nitrides due to their unique characteristics among III-V compounds. These nitrides are known for their stability at high temperatures, short bond lengths, low compressibility, and high thermal conductivity. They are promising for spintronic

* Corresponding author.
E-mail address: mgupta@csr.res.in (M. Gupta).

https://doi.org/10.1016/j.apsadv.2025.100884
Received 2 June 2025; Received in revised form 12 October 2025; Accepted 16 October 2025
Available online 27 October 2025

and optical devices [14], particularly in high-frequency and high-power electronic applications. Among the group-III nitrides, AlN stands out as a prominent compound within the III-V family. It offers exceptional physical, chemical, and mechanical properties, making it ideal for electro-optical devices that operate under extreme conditions [15]. However, recent studies suggest that incorporation of Al can improve the hardness and oxidation resistance of the VAlN coating [16]. Metastable cubic-TMAlN compounds [17], are achievable through physical vapor deposition because of kinetically limited low temperature growth and the dynamic low-energy ion irradiation in the near-surface region [18].

VAlN, which has the same structure as TiAlN, has been found to have a lower coefficient of friction [19] compared to TiAlN coatings [20]. Both TiAlN and VAlN form metastable solid solutions [9,21,22] and can be easily synthesized using direct-current magnetron sputtering (dcMS) [23] or high-power impulse magnetron sputtering (HiPIMS) [24]. In general, when Al is added to face-centered cubic (fcc) TiN or VN, metastable fcc-TiAlN or fcc-VAlN solid solutions are typically formed. As a result, both hardness [23] and oxidation resistance [25] are significantly enhanced as compared to the binary TiN or VN. Considering these characteristics, it is essential to investigate the formation of the metastable phase and to establish the maximum solubility limit (x_{max}) of Al in $TM_{1-x}Al_xN$. A few studies have been conducted to address these objectives, e.g. Rovere et al. reported an x_{max} value of 0.54 [26], whereas Zhu et al. found a range of $0.52 \leq x_{max} \leq 0.62$ [23].

Using an advanced sputtering method like HiPIMS [22] to further boost x_{max} in fcc-$V_{1-x}Al_xN$ is found to be an effective strategy. In this context, it is noteworthy that Greczynski et al. used hybrid co-sputtering, powering the V target with a dcMS generator and the Al target with a HiPIMS generator, to deposit fcc-$V_{1-x}Al_xN$ films with x_{max} of up to 0.65. In contrast to the plethora of experimental studies, there are very few theoretical and computational works focusing on x_{max} in fcc-$V_{1-x}Al_xN$. The VAlN system is relatively less explored, with only few reports [19,22–24] yet potentially useful predominantly due to the combination of high hardness and low friction coefficient, which makes it a promising candidate for applications as a wear-resistant coating in deep drawing of high-strength steels.

The motivation of our work is to investigate the metastable phase formation and to find the x_{max} in fcc-$V_{1-x}Al_xN$. In this work, we deposited $V_{1-x}Al_xN$ thin films by varying Al concentration (x = 0, 35, 60, 71, 84, and 100 %) at constant nitrogen partial pressure (RN_2 = 25 %) at 300 K. Films deposited at x = 0 and 100 % are used as a reference and correspond to binary VN and AlN, respectively. To understand the role of Al in the metastable phase formation, $V_{1-x}Al_xN$ thin films were characterized using grazing incidence x-ray diffraction (GIXRD). The electronic structure of the films was probed by x-ray absorption spectroscopy (XAS). The N K-edge spectra show a shift towards the lower binding energy as Al concentration increases. Whereas the structural stability of the doped films is elucidated by x-ray absorption near edge structure (XANES) measurement. We found that on increasing the Al concentration, finite charge transfer takes place which is investigated by the core-level hard x-ray photoelectron spectroscopy (HAXPES). Films deposited at x = 71 % and above show semiconducting behaviour due to higher amount of Al doping. The hardness of $V_{1-x}Al_xN$ thin films acquired by nanoindentation reveals an increment in the hardness on increasing Al concentration. The result obtained through this work establishes $V_{0.29}Al_{0.71}$ N having a structure similar to VN but it is a semiconductor with band gap of 3.4 eV and having a hardness similar to that of AlN.

2. Experimental details

$V_{1-x}Al_xN$ thin films (x = 0, 35, 60, 71, 84, and 100 %) were deposited on Si (100), SiO_2 and glass substrates at room temperature (300 K) using a reactive direct current magnetron sputtering (dcMS) process (Orion 8, AJA Int. Inc.). V (99.99 %) and Al (99.99 %) target of diameter 3inch were sputtered using argon and nitrogen gas mixture (both 5 N purity) in which Ar and N_2 flows were kept fixed at 37.5 and 12.5 sccm, respectively. The base pressure in the vacuum chamber was about 2×10^{-7} Torr and the working pressure was about 3×10^{-3} Torr. The thickness of the thin films was determined using Bruker D8 Discover x-ray reflectivity (XRR) system equipped with Cu-Kα x-ray source. Experimental XRR patterns were fitted using the Parratt-32 software package [27]. The typical thickness of samples was kept around 200 nm and the composition was controlled by varying the power of individual sources. The optimization details of $V_{1-x}Al_xN$ samples are provided in the supporting information (SI). The composition of the $V_{1-x}Al_xN$ thin films was analyzed using energy dispersive x-ray spectroscopy (EDS) with an Oxford Instruments system. This system is equipped with a liquid nitrogen cooled analytical drift detector and can detect elements from boron and above. The detector had an active area of $10mm^2$ and used an ultrathin polymer window. The distance between sample to detector was 9 mm. A detailed description of the method used to calculate the Al concentration, along with the corresponding EDS spectrum is provided in the SI. The Al concentrations determined from EDS analysis in the $V_{1-x}Al_xN$ thin films are x = 0, 35, 60, 71, 84, and 100 %.

To investigate the crystal and the local electronic structure, GIXRD and soft XAS measurements were carried out respectively at BL-02 [28] and BL-01 [29] beamlines of Indus-2 synchrotron radiation source at RRCAT, Indore, India. GIXRD measurements were performed using x-rays of energy 15 keV and the color of the deposited thin films measured using benchtop spectrophotometer (DS-36D) in the wavelength range of 360–780 nm. Soft XAS measured using a surface sensitive total electron yield (TEY) detection mode. Extended x-ray absorption near structure (EXAFS) measurements and HAXPES measurements were carried out at P64 [30] and P22 [31] beamlines of Petra III synchrotron radiation source at DESY, Hamburg, Germany. In the HAXPES measurement the photon energy was 6 keV with an energy resolution of 40meV. The detector used was SPECS Phoibos 225HV hemispherical analyser with a delay line detector. The base pressure was 10^{-9} mbar. The incident angle and electron emission angle was 5° and 45° respectively. CASA XPS software was used for analysis with shirley as a background subtraction. In the XAS and HAXPES measurements, the sample was placed on a copper block, and silver paste was used to make electrical contact with the block. XAS data was processed in Athena software [32] with pre and post-edge normalization and fitting of the Fourier Transform (FT) spectra. The optical data of the samples were recorded by Perkin Elmer, Lambda750 UV–Visible spectrophotometer with double beam monochromator in the spectral range of 200–858 nm at room temperature. Nanoindentation tests (M/s. Anton Paar, Switzerland) were carried out using a Berkovich diamond indenter tip to measure the hardness and elastic modulus of the samples. The loading and unloading rate were 0.32mN/min with a maximum load of 0.16mN. The number of indentations taken for averaging was 9 per sample. The resistivity (ρ) was measured using a four-probe method in a PPMS (Quantum Design). The surface morphology was examined using a Nanoscope V Atomic Force Microscopy (AFM) system (Bruker bioscope resolve). The obtained data for resistivity and AFM is presented in the SI. All characterizations, except for UV–Vis and EXAFS, were conducted on Si (100) substrates. UV–Vis and EXAFS measurements were performed on samples deposited on fused quartz (SiO_2) substrate.

3. Results and discussion

3.1. GIXRD and color measurements

Synchrotron GIXRD patterns of $V_{1-x}Al_xN$ samples deposited on Si (100) substrates with x = 0, 35, 60, 71, 84, and 100 % are shown in g. 1 (a). For comparison, the reference XRD pattern of fcc-VN (JCPDS card no 00–035–0768) and hcp-AlN (JCPDS card no 00–003–1144) have also been included. As can be seen, x = 0 and 100 % samples match well with

fcc-VN and hcp-AlN. The lattice parameter (LP) of VN and AlN samples calculated from the most intense peaks comes out to be 4.12±0.01 Å for VN and $a = b = 2.85\pm0.01$ Å and $c = 4.97\pm0.01$ Å for AlN. These values match very well with their theoretical LPs. In case of VN, generally growth along the (111) plane has been observed in thin films deposited using reactive magnetron sputtering [33]. The addition of Al at 35, 60, and 71 %, does not affect the growth of VN as illustrated in the zoomed view of XRD pattern shown in g. 1(b). Even for the highest Al content (x = 71 %) sample, it is hard to identify clearly any contribution of the crystalline B4 structured AlN phase (hcp-AlN), due to the proximity of the (101) plane of AlN to the (111) plane of VN [23]. In this study, we deposited the films at room temperature (300 K), which acted as a kinetic barrier, preventing the separation of the crystalline hcp-AlN phase. This can be understood in the following terms: The higher Al solubility observed in our room temperature deposited $V_{1-x}Al_xN$ films compared to elevated-temperature studies can be attributed to non-equilibrium growth conditions and kinetically driven mechanisms unique to room-temperature physical vapor deposition (PVD). Several studies [22, 26] have demonstrated that the solubility of Al in the cubic VN lattice can be significantly extended under highly non-equilibrium conditions, especially due to limited surface diffusion and the suppression of phase separation during room-temperature deposition. In particular, at low substrate temperatures, adatoms have insufficient mobi-lity to reorganize into thermodynamically stable phases such as hexagonal wurtzite AlN. This favours the kinetic trapping of Al atoms in the cubic VN lattice, resulting in a supersaturated solid solution. At higher temperatures, enhanced diffusion promotes phase separation and formation of equilibrium Al-rich secondary phases, which naturally limits the Al solubility in the cubic structure. Thus, our findings are consistent with literature on metastable phase formation, and the elevated Al solubility in our room-temperature films can be rationalized by the combined effect of kinetic suppression of phase segregation under non-equilibrium growth conditions. However, when the amount of Al was increased to 84 %, a mixture of VN and AlN phases can be seen. This result is inline with previous studies where it was found that the Al addition in TiN or VN does not significantly affect the growth of host TiN [34] or VN [35] Fig. 1.

Table 1 compares the available literature of $V_{1-x}Al_xN$ system in which samples have been deposited using different deposition methods and various temperatures. Here, it is interesting to find that even though our sample have been deposited at room temperature only, the maximum Al solubility range was found to be 71 % as opposed to smaller values obtained in samples deposited at a higher temperature. The

Table 1
$V_{1-x}Al_xN$ thin film grown using different deposition methods at various substrate temperatures (T_S) showing range of Al solubility and x_{max} value; Here, dc/rf MS = direct current/radio frequency (dc/rf) magnetron sputtering (MS), HiPIMS = High power impulse magnetron sputtering.

Method	T_S (K)	Al range	xmax	ref.
dc bias	623	–	–	[36]
dc bias	723	0.2–0.85	0.54	[26]
V-dc/Al-rf	573	0–0.62	0.52	[23]
HiPIMS	773	0.17–0.74	0.65	[22]
rfMS	473	0–0.38	0.38	[35]
dc bias	823	0.11–0.91	0.62	[37]
dcMS	300	0–0.84	0.71	this work

optical color of the Al-doped VN thin films was evaluated using a spectrophotometer in transmission mode, which also provided the corresponding color coordinates and is shown in g. 1. Color measurements were performed using the CIELAB color space, as standardized by the Commission Internationale de l'Eclairage (CIE) [38]. In this color space, colors are described using three Cartesian coordinates: L* denotes the lightness of the color, ranging from 0 (ideal black) to 100 (perfect white); a* indicates the position on the red-green axis, with positive values corresponding to red and negative values to green; and b* represents the yellow-blue axis, where positive values indicate yellow and negative values indicate blue. The color coordinate of $V_{1-x}Al_xN$ samples are reported as follows: for 100 % Al, L*= 89.5, a*=0.74, b*=3.05; for 84 % Al, L*= 80.22, a*= 0.13, b*= 3.94; for 71 % Al, L*= 73.1, a*= −0.69, b*= 2.58; for 60 % Al, L*= 72.06, a*= −0.94, b*= 1.75; for 35 % Al, L*= 72.53, a*= −1.14, b*= 0.9 and for 0 % Al, L*= 72.21, a*= −1.14, b*= 0.9. Here, it can be seen that on increasing Al content the value of L* gradually increased from 72.06 to 89.5 which represents a clear transition from dark grey to white (transparent). This transition can be attributed to the incorporation of AlN, a wide-bandgap semiconductor (≈6 eV), known for its transparency in the UV–visible region making it a promising candidate for optoelectronic devices. This also confirm the structural changes of $V_{1-x}Al_xN$ thin films on increasing Al content.

3.2. X-ray absorption spectroscopy measurements (XANES and EXAFS)

Fig. 2(a) shows V $L_{2,3}$-edges compared with the reference V_2O_3 sample which corresponds to the transition of V-2p to V-3d states. As observed, the V L_3 and L_2 edges in V_2O_3 and $V_{1-x}Al_xN$ samples are

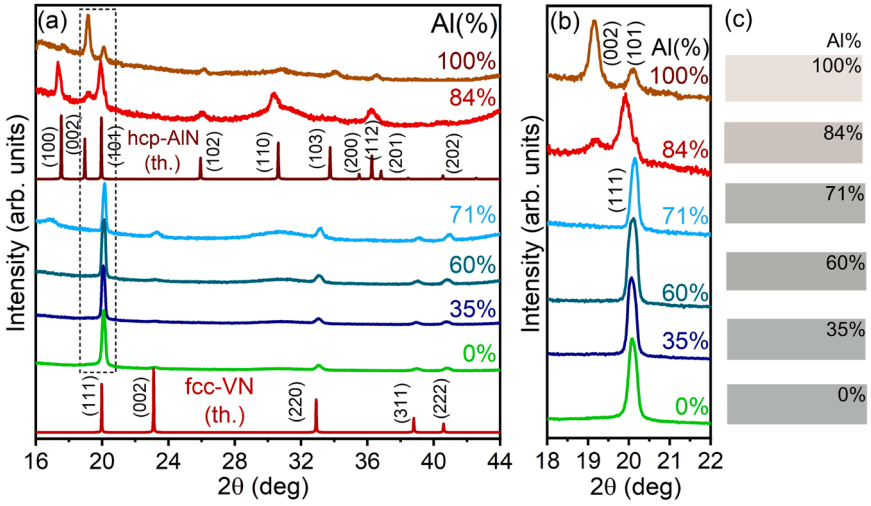

Fig. 1. Grazing incidence x-ray diffraction pattern of $V_{1-x}Al_xN$ samples measured at BL-02 beamline of Indus-2 at beam energy of 15 keV (a) Enlarged view of selected region of the diffraction pattern (b) and simulated optical color with corresponding color coordinates of the thin films displayed adjacent to the diffraction pattern (c).

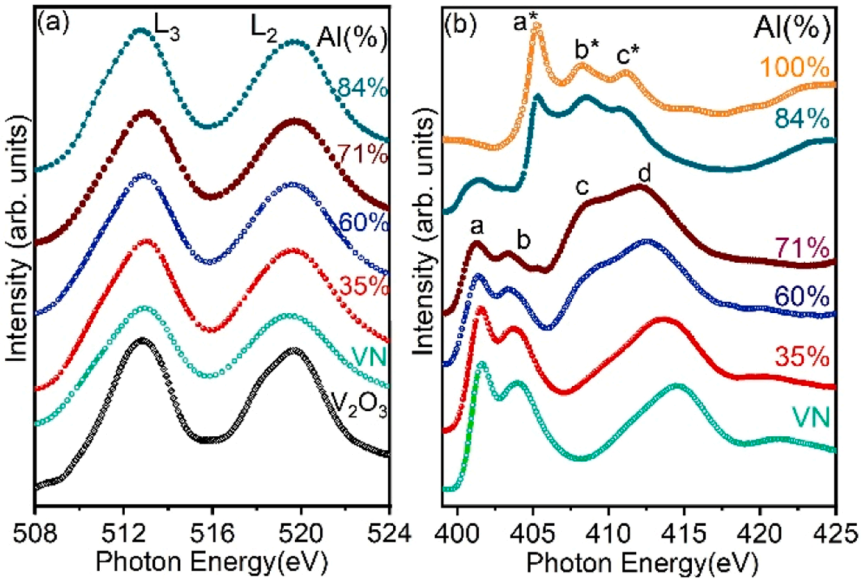

Fig. 2. Normalized soft x-ray absorption spectra of V $L_{3,2}$edges (a) and N K-edge (b) of $V_{1-x}Al_xN$ thin lms samples.

almost similar, confirming the V^{3+}charge state. The N K-edge XAS spectra, shown in Fig. 2(b), reveal interesting insights into the unoccupied electronic states, especially probing the N-2p density of states (DOS). A sharp transition arises for all samples around a threshold of 401 eV. We observe multiple peaks in the spectra labelled as *a, b, c, d, a*, b**, and *c**. Here, each characteristic peak represents the transition from N-1 s to electronic sub-bands present above the Fermi level. In the case of metals, the Fermi level lies somewhere between the overlapped region of both bands and the features in the XAS spectra are the result of filling of electrons in the DOS above Fermi level. In early TMNs, TM has an octahedral coordination with N. Metal d orbitals split into t_{2g} and e_g levels because of the crystal field which are further hybridized with N-2p orbitals. The V Ll-edge and N K-edge of VN films are consistent with previous reports [39].

In Fig. 2(b), the feature *a* and *b* arise due to the hybridized N-2p and t_{2g} and e_g levels of V 3d orbitals, respectively. Feature *d* arises due to higher order hybridization between N-2p and V-4s+4p orbitals. It is quite interesting to note that on increasing Al concentration a shift towards the lower energy region in feature *d* is observed. The shift in overall spectra towards the lower energy region signifies the lower oxidation state and the enhancement of covalent bonding. The significant change observed with Al incorporation into VN can be attributed to the simultaneous modification in the electronic structure. In the binary VN configuration, the electronic structure is primarily characterized by the overlap of V3d-N2p orbitals, leading to sp^3d^2 hybridization, which is consistent with the literature [40]. Upon incorporating Al, the bonding nature remains unchanged, and strong sp^3d^2 hybridization exists between Al and N.

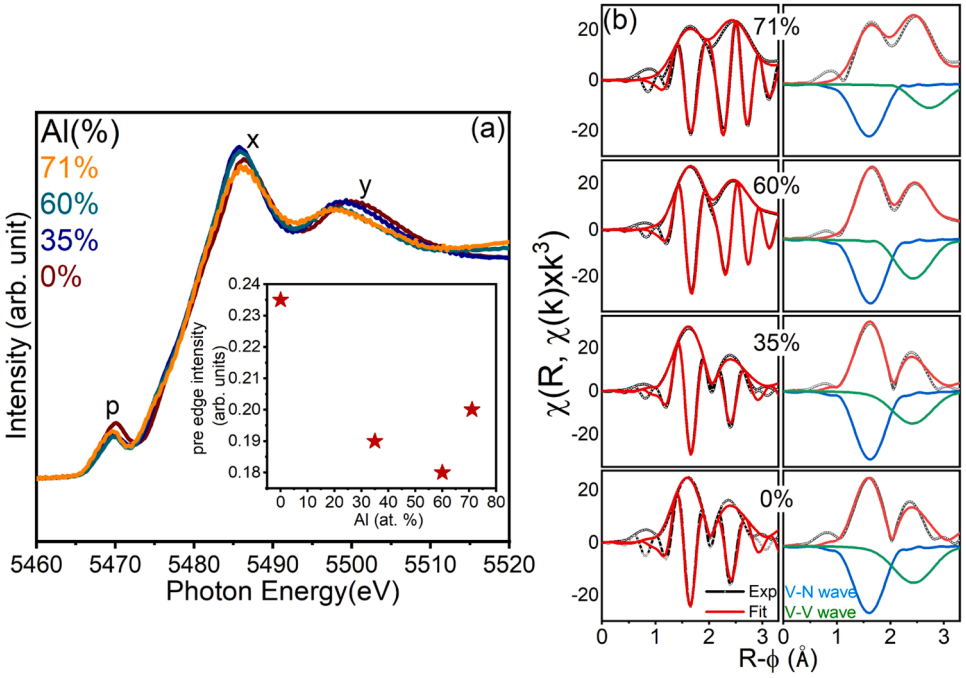

Fig. 3. XANES spectra of V-K edge (a) Fourier transform moduli ($|\chi(R)|$), real component ($Re|\chi(R)|$) of EXAFS spectra plotted against phase shifted (ϕ) interatomic distance (b) of $V_{1-x}Al_xN$ thin film samples.

The N K-edge of 84 at. % sample and AlN sample has also been measured and it can be seen that there is a significant shift in the edge position compared to VN sample. Such a shift is observed because of the semiconducting behaviour of the AlN. Both bands are separated by a finite energy gap (≈4–6 eV) which is clearly seen from the N K-edge spectra.

Fig. 3(a) shows the XANES spectra taken at the V K-edge for $V_{1-x}Al_xN$thin films. The edge position, measured at 50 % absorption for all samples, is 5467 eV (±0.3). Interestingly, a pre-edge peak which arises due to the electric-dipole transition can be seen in all samples.

The features marked as *x* and *y* arise from electronic transitions from the V 1 s core level to the V 4*p* and transition to higher *np* states followed by the dipole selection rules [41]. In general, the electric quadrupole transition from the 1 s to the 3*d* orbital can also produce a pre-edge peak, however, the likelihood of such a transition is much lower as compared to the dipole transition. The pre-edge feature *p* arises because 1*s*-3*d* is dipole forbidden transition. It becomes dipole allowed due to 3*d*-4*p* mixing and metal 3*d* and ligand 2*p* orbital overlapping [42]. Now in the inset of Fig. 3(a) we have plotted *p* feature intensity as a function of Al (%) doping. The intensity of *p* gets reduced with Al (minimum for 60 at %) doping and again increases for 71 at %. The decrease in the pre-edge intensity, is likely related to incorporation of Al as well as the evolution of defect structures. The minimal change in XANES features up to 71 % Al suggests that the major phase remains fccVAlN, which is consistent with XRD findings. To further investigate the local atomic environment, we analyzed the Fourier-transformed EXAFS spectra (Fig. S6 (a) of SI) for samples up to 71 % Al. The first two coordination shells correspond to V-N and V-V interactions. For the 60 % and 71 % Al samples, significant spectral broadening is observed between 2 3 Å. When fitting the EXAFS data using only two shells (V–N and V–V), residuals remain high, particularly for the higher Al concentrations. By including a V–Al shell in the fit, assuming Al substitution at V sites in the fcc-VN lattice, we observed significant improvement in the fit quality. This strongly supports the incorporation of Al into the lattice. This is also supported by the observed shift in the absorption edge to lower energies. Overall, the observed variation in pre-edge intensity can be attributed to a combination of Al substitution and evolving defect concentration. Since the primary focus of this study is the formation of the fcc-VAlN phase, we plan to carry out future work with finer Al concentration increments to gain more insight into the evolution of residual phases and their effects on the structural, electronic, mechanical, and optical properties.

It is well-known that the intensity of the pre-edge peak is a useful indicator of the local coordination in various samples. Typically, the geometry of ion affects the amount of p-d mixing, which controls the intensity of a peak. Stronger p-d mixing leads to a more intense pre-edge peak, especially when the local coordination is distorted from the symmetric octahedral geometry and is strongest in tetrahedral coordination. For equiatomic TMN, it has been suggested that the compound can crystallize in either the NaCl-type or ZB-type structure, which di er in local coordination. It is well-known that V and N are bonded in the octahedral coordination which is observed in the NaCl type structure. Least-square fitting of the EXAFS data was performed to obtain the metrical parameters. The representative plots and the obtained results are presented in g. 3 (b) and Table 2. Here, R is obtained atomic pair distance, N is coordination number, σ is root mean square displacement and ΔE_0 is energy shift parameter. The metrical parameters obtained from the fitting correspond to the V N and V-V shells. For the V-N shell, all metrical parameters remain consistent up to 71 at. % Al doping. However, for the V-V shell, the coordination number (N) shows inconsistency at 60 and 71 at. % Al doping. To maintain the consistency in the fitting model two samples (0 and 35 at. %) are fitted by keeping fixed N at 12 and for the 60 and 71 at. % samples the Al is substituted on V site and the total coordination was constrained to 12. At higher Al concentrations, the potential formation of small V-metal clusters may disrupt the periodicity of V-V bonds within the VN matrix. Such cluster formation has been previously observed in ternary transition metal nitrides

Table 2
Metrical parameters derived from non-linear least square tting of EXAFS data at V K-edge in $V_{1-x}Al_xN$ thin lms with $x = 0$, 35, 60 and 71 % measured. Here, R is the obtained atomic pair distance, N coordination number, σ root mean square displacement and ΔE_0 is energy shift parameter.

Shell and parameters	0 %	35 %	60 %	71 %
V-N R(Å)	2.02±0.01	2.03±0.01	2.04±0.01	2.03±0.01
N	5.5 ± 0.3	5.7 ± 0.3	5.6 ± 0.5	5.4 ± 0.3
σ	0.09±0.01	0.08±0.01	0.09±0.01	0.11±0.01
ΔE_0	4.7 ± 0.2	4.6 ± 0.2	4.5 ± 0.2	4.5 ± 0.2
V-V R(Å)	2.83±0.01	2.81±0.01	2.8 ± 0.01	3.1 ± 0.01
N	12±2.1	12±1.9	5.8 ± 0.6	5.4 ± 1.5
σ	0.18±0.01	0.18±0.01	0.16±0.02	0.17±0.03
ΔE_0	4.7 ± 0.2	4.6 ± 0.2	4.5 ± 0.2	4.5 ± 0.2

deposited via magnetron sputtering [43]. In our current work, we observe that with Al doping up to 84 at. %, the pre-edge peak in the XANES spectra shifts significantly to lower energies compared to the 0 at. % Al sample, suggesting the formation of a nitrogen-deficient phase. However, the XANES features remain distinct from those of pure V metal (Fig. S6 (b) of SI), indicating that the presence of metallic V clusters cannot be unambiguously confirmed. Alternatively, the formation of V-Al alloys or other V-Al-N phases could be contributing to limited grain growth. These phases are likely metastable and remain largely uncharacterized in existing literature, making their precise identification through XRD and XAFS particularly challenging. Furthermore, the limited number of observable XRD peaks, combined with the potential presence of composite or amorphous Al N phases, complicates the structural analysis. This makes it difficult to assign a definitive crystal structure to the samples at high Al doping levels. In this work there is limitations of the current characterization techniques in resolving small V-metal clusters from V-Al-N configurations. Additionally, a more detailed investigation with finer variations in Al doping is needed to better understand the evolution of these phases.

3.3. Hard X-ray photoelectron spectroscopy

Core-level HAXPES measurements were performed in the $V_{1-x}Al_xN$ samples. Various regions such as V2p, N1s, and Al2s are measured and shown in g. 4 (a), (b) and (c), respectively. A reference Au sample has been used for calibration of the energy scale. Fig. 4(a) shows the component analysis of V-2p core-level spectrum showing various features. The binding energy (BE) of feature A centered at 513.4 eV and feature A* centered at 520.8 eV correspond to the V-N feature of spin orbit $V2p_{3/2}$ and $V2p_{1/2}$ split states, respectively. Previous studies have shown that the BE peak of pure V is centered at 512.3 eV [44], which is lower than the value observed for our VN film ($\Delta V2p_{3/2} = 1.1$ eV). This shift of 1.1 eV between V and VN samples is attributed to the higher oxidation state of vanadium in VN. The BEs of feature A remains centered around 513.4 eV up to 60 at. % Al. However, with further Al incorporation at 71 at. % and 84 at. % the BE shifts to 514.3 eV and 515 eV, respectively, indicating a significant increase. This shift can be explained by the increasing Al content, which enhances covalent bonding in the system and thus binding energy increases. Moreover, each spin orbit split state exhibits satellite features B (at ≈ 516.3 eV for nearly all samples) and B* (at 523.6 eV). The existence of these satellite features on the high binding energy side of the V $2p_{3/2}$ and V $2p_{1/2}$ transitions has been well documented by Zhu et al. [23]. Feature C and C* centered at ≈514.6 eV and ≈521.8 eV respectively indicate the V-O feature of Al-doped VN thin films.

The N 1 s core-level spectrum is presented in Fig. 4(b), displaying features X and Y representing N-V and N—O feature respectively.

Feature X, centered at 397 eV, corresponds to N 1 s peak, while feature Y, at 398.6 eV, appears as a shoulder. The BE of feature X is consistent with the values for stoichiometric VN [45]. As the Al concentration increases till 71 at. %, the N 1 s peak shifts toward lower

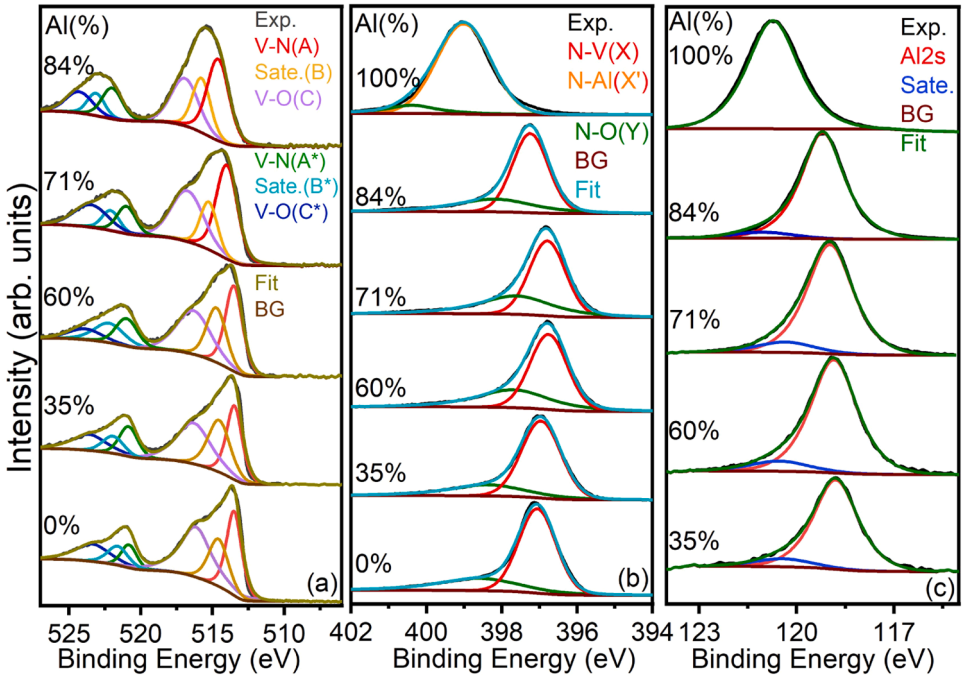

Fig. 4. Core-level HAXPES spectra of the $V_{1-x}Al_xN$ sample (a) V 2p region (b) N 1 s region and (c) Al 2 s region with peak component analysis.

binding energy and after it shift to higher BE. This shift is also observed for V-Al-N coating studied by Zhu et al. [23]. Such shift to lower BE indicates a finite charge transfer between V and N atoms, which is also reflected in the V 2p peak, as it shifts to higher BE. This behaviour occurs while the film maintains its fcc crystal structure up to 71 at. % Al. Additionally, this trend is observed in the N K-edge measurements also, where a structural change to w-hcp occurs at 84 at. % Al. Conversely, feature Y could be a result of surface oxidation [46,47], which leads to the formation of N O bonds [48–50]. Additionally, we have observed the feature X′ representing N-Al peak for the pure AlN sample, while in all V-Al-N samples the N-V feature is observed. This can be explained as follows: the binding energies of the N 1 s peaks in pure VN and AlN are significantly different, but when both Al and V are present in the same sample, an intermediate binding energy appears, closer to that of pure VN. Therefore, for the pure AlN sample, the N-Al peak is specifically assigned which is also consistent with the reports [51].

Further the Al2s region is also measured and is shown in g. 4 (c). As can be seen a significant change can be observed while increasing Al concentration. The Al2s peak centered at 118.eV is consisted till 71 at. % Al and then it shifts to higher BE at higher Al concentration. Wiesing et al. also reported satellite feature in Al 2 s region at higher BE [52], which can be also seen in our spectra. However, for V-Al-N thin films it is very rare to see Al2s spectra in XPS measurement. For the pure AlN sample only one peak is observed after fitting which has been well documented in previous XPS studies [53]. Overall, it can be concluded that the observed shift in all spectra is due to increasing Al concentration due to which a finite charge transfer takes place between the atoms and amount of covalent bond increases which is also reflected in the hardness as shown later.

3.4. UV–VIS measurements

To examine the optical properties of $V_{1-x}Al_xN$ samples, UV–Vis measurements were performed on samples deposited on fused quartz substrate (one side polished) in reflection mode. The corresponding reflectance and the band gap determination is shown in the fig. S7 and S8 of SI respectively. Resistivity measurements has also been done for all samples and are provided in Fig. S1 of the SI. VN being metallic (Al = 0 %) has a resistivity (at 300 K) value of 995 $\mu\Omega$cm and it increases to 2699 $\mu\Omega$cm (for Al = 35 at. %), 5877 $\mu\Omega$cm (for Al = 60 at. %). These results indicate that the samples with 0, 35, and 60 % Al exhibit metallic behaviour. However, with 71 % Al or higher, a transition to a semiconducting state can be observed characterized by a distinct optical bandgap. It can be seen in the reflectance spectra that the interference fringes (oscillations) observed while measurement. These fringes arises due to multiple reflections within the thin film. When incident light partially reflects from the air/film and film/substrate interfaces, the reflected beams interfere constructively or destructively depending on the optical path difference between them. This thin-film interference produces periodic oscillations. Similar interference fringes have been already reported in TiO_2 films [54]. The optical band gap of the films was estimated using the Kubelka-Munk function. As described by Kubelka and Munk [55], the reflectance spectra can be converted into corresponding absorption spectra by applying the Kubelka-Munk equation, $F(R) = (1\text{-}R)^2/2R$, where R is the measured reflectance and F(R) is proportional to the absorption coefficient (α). Replacing the value of α in the Tauc relation: $\alpha h\nu = A(h\nu - E_g)^n$ [56], where $h\nu$ represents photon energy, E_g is the optical bandgap, and A is a proportionality constant. We get $(F(R).h\nu) = A(h\nu - E_g)^n$ where n indicates the nature of the electronic transition (direct or indirect) [57]. According to the Tauc method, a linear fit is applied to the main absorption edge. In addition, a linear baseline was fitted to the data below the fundamental absorption region to serve as a reference for determining the slope. The intersection point of the two fitting lines [57] gives the estimated band gap energy, as shown in Fig. S8 of SI Table 3.

Table 3
Hardness analysis of $V_{1-x}Al_xN$ thin film. Here H = Hardness, E = Elastic Modulus, H/E = resistance of material to elastic strain and H^3/E^2 = resistance of material to plastic deformation.

Al %	H (GPa)	E (GPa)	H/E	H^3/E^2
0	7.13	272.43	0.026	0.004
35	12.02	406.01	0.029	0.011
60	16.81	203.93	0.082	0.114
84	17.38	331.84	0.052	0.047
100	21.89	188.14	0.116	0.296

In this context, it is to be mentioned that AlN exhibits a direct bandgap of 6.2 eV [58]. However, for our samples the trend was linear in nature with a maximum value of 5 eV for pure AlN sample, 4.4 eV for 84 % Al and reduces to ≈ 3.4 eV for 71 % Al. Thus, the variations in the bandgap value in AlN can be inferred primarily to the contribution of defects. For 71 % and 84 % Al sample the bandgap reduced due to the presence of V-atoms. Similar trend is also observed for Al doped TiN samples [59].

3.5. Nanoindentation measurements

Nanoindentation system was used to measure the hardness of $V_{1-x}Al_xN$ thin films as a function of Al concentration. Fig. 5(a) and (b) illustrate the indentation hardness (H) and elastic modulus (E) for $V_{1-x}Al_xN$ films with $x = 0$ to 100 at. %. Following the indentation 'thumb rule', to accurately measure film hardness and minimize substrate effects, indentation was conducted at depths less than one-tenth (1/10*th*) of the total film thickness, by Buckel's one-tenth rule [60]. In this study, the $V_{1-x}Al_xN$ films have a thickness of approximately 200 nm. The H and E of these films were measured at a depth of ≈20 nm, in accordance with the one-tenth rule. As can be seen from Fig. 5(a) the hardness of films increases gradually with $x = 0$ to 60 at. %. In general, the hardness is determined by microstructure, orientation and the crystallite size of the thin film. In this study, we found that the crystallite size (19.24±1 nm for VN, 19.16±1 nm for 35 at. % Al, 18.55±1 nm for 60 at. % Al and 18.63±1 nm for 71 at. % Al) decreases with the increase in Al concentration. According to the Hall Petch relation [61], a reduction in crystallite size results in increased hardness. Thus, the indentation hardness increased from 7.13 GPa to 16.81 GPa as the Al concentration increases from 0 to 60 at. % and then saturates at 71 and 84 at. % samples. The significant increase in hardness observed in ternary V-Al-N films compared to the binary VN system is primarily due to solution strengthening. Vacancies are commonly found in binary metal nitrides deposited via magnetron sputtering. The addition of Al into the vacancy-stabilized VN likely introduces a larger number of covalent bonds.

The ratio of hardness H and E i.e., H/E and H^3/E^2 ratios are well-known mechanical parameters in hard films, since the H/E ratio is considered as the material ability of elastic strain resistance and H^3/E^2 ratio is defined as the resistance of material to plastic deformation. The coatings with value $H/E > 0.1$ have enhanced toughness, which relates to its ability to withstand plastic deformation. H/E ratio of AlN is greater than 0.1, which shows the high surface toughness. The highest H/E ratio for VAlN is of $x = 60$ at. % and 71 at. %, which shows that on increasing the Al % the hardness increases. The materials having high hardness and lower elastic modulus present great resistance to plastic deformation. This behaviour is expressed by H^3/E^2 ratio. The highest value of H^3/E^2 within fcc-structure is of 60 at. % and 71 at. % samples which again shows the resistance to plastic deformation. The gradual increase in hardness observed with higher Al content in our V1-xAlxN thin films can be explained by the well-known solid solution strengthening mechanism. When Al atoms substitute V in the lattice, their smaller size and different electronic structure introduce local strain fields [62]. These distortions make it harder for dislocations to move, thereby increasing the material's resistance to deformation [63]. Furthermore, in transition metal nitrides (TMNs), the hardness also depends strongly on the covalent-metallic bonding character [64]. Al incorporation modifies the electronic structure, increasing covalent-metallic bonding, which in turn can increase the resistance to shear and deformation, contributing to hardness enhancement.

4. Conclusion

In conclusion, this study demonstrated the ability to deposit the fcc-VAlN phase with a higher x_{max} value without requiring elevated temperatures during the growth process. The effect of Al content on the microstructure, chemical states, as well as the mechanical and optical properties, was examined using XRD, XAS (including XANES and EXAFS), HAXPES, UV–Vis, and nanoindentation measurements. At a significantly higher Al content (x_{max}), fcc $V_{1-x}Al_xN$ solid solution was identified, and a metastable B1 structure was stabilized in the ternary $V_{1-x}Al_xN$ thin films. Structural measurements revealed the cubic phase with the highest Al content at $x = 0.71$. However, beyond $x = 0.71$, evidence of the h-AlN phase was identified through XRD and XAS analyses. As the Al content increased up to $x = 0.84$, the growth structure evolved, becoming coarser, as observed from AFM analysis. Simultaneously, XAS and HAXPES analyses revealed charge transfer and an increase in covalent bonding between atoms. The optical bandgap ranged from 3.4 to 5 eV for $x = 0.71$–1, while the hardness increased with rising Al concentration, reaching a peak value of 16.8 GPa for fcc-VAlN. It is therefore anticipated that with further fine-tuning the Al concentration at high temperatures, it should be possible to achieve an even higher x_{max} value during the growth process.

CRediT authorship contribution statement

Amit Kumar Verma: Writing – review & editing, Writing – original draft, Visualization, Validation, Software, Methodology, Investigation, Data curation. **Rachana Gupta:** Writing – review & editing, Supervision, Project administration, Methodology, Investigation, Funding acquisition. **Pooja Gupta:** Writing – review & editing, Supervision, Methodology. **Sanjay Rai:** Writing – review & editing, Supervision, Project administration, Methodology. **Shashi Prakash:** Writing – review & editing, Validation, Supervision, Project administration. **Akhil Tayal:** Writing – review & editing, Validation, Resources, Methodology, Investigation. **Andrei Gloskovskii:** Writing – review & editing,

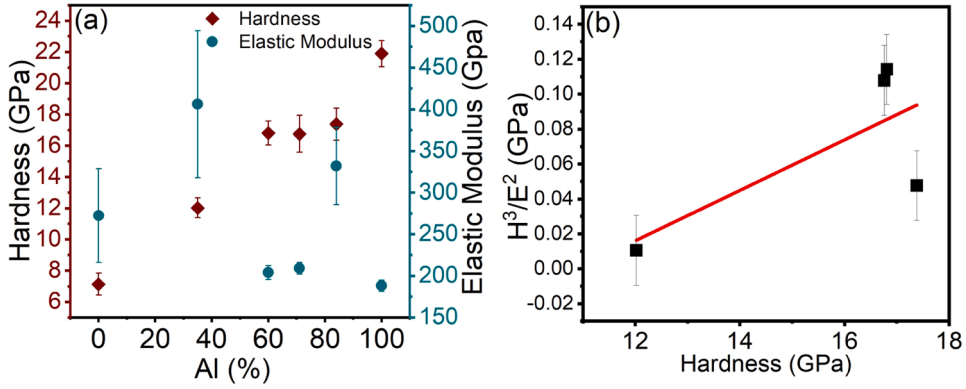

Fig. 5. Nano-indentation hardness and modulus of $V_{1-x}Al_xN$ thin lms coating (a) with error bars and the ratio of (H^3/E^2) depicting resistance to plastic deformation of $V_{1-x}Al_xN$ thin lm as a function of hardness (b).

Validation, Resources, Methodology, Investigation. **R. Ramaseshan:** Writing – review & editing, Validation, Resources, Methodology. **Parveen Garg:** Writing – review & editing, Validation, Methodology. **Uday Deshpande:** Writing – review & editing, Validation, Methodology. **Mukul Gupta:** Writing – review & editing, Validation, Supervision, Resources, Project administration, Methodology, Investigation, Funding acquisition, Conceptualization.

Declaration of competing interest

The authors declare that they have no known competing financial interests or personal relationships that could have appeared to influence the work reported in this paper.

Acknowledgements

A part of this work has been carried out through ANRF CRG project no CRG/2023/000946. Authors (AKV and RG) are sincerely thankful to UGC-DAE CSR, Indore for providing financial support through CRS/2021–22/01/377 project. AKV is deeply grateful to S. Kalal for insightful discussions and technical expertise. We would like to acknowledge L. Behera for cooperation during various measurements, R. Rawat and R. Joshi for resistivity measurements. We also acknowledge R. Venkatesh and M. Gangrade for AFM measurements, R. Sah and A. Wadikar for soft XAS measurements at BL-01, Indus 2, RRCAT, Indore, India. A part of this work is supported through India-DESY project. We also thank S. Tokekar, V.G. Sathe and A.J. Pal for their kind support and constant encouragements. AKV is also thankful to Ashish, Nikita, and Akshaya for their help in experiments and discussions.

Supplementary materials

Supplementary material associated with this article can be found, in the online version, at doi:10.1016/j.apsadv.2025.100884.

Data availability

Data will be made available on request.

References

[1] D.D. Kumar, N. Kumar, S. Kalaiselvam, S. Dash, R. Jayavel, Wear resistant super-hard multilayer transition metal-nitride coatings, Surf. Interfaces. 7 (2017) 74–82. ISSN 24680230.
[2] D.D. Kumar, N. Kumar, S. Kalaiselvam, S. Dash, R. Jayavel, Substrate effect on wear resistant transition metal nitride hard coatings: microstructure and tribo-mechanical properties, Ceram. Int. 41 (8) (2015) 9849–9861. ISSN 0272-8842.
[3] H. Ju, S. He, L. Yu, I. Asempah, J. Xu, The improvement of oxidation resistance, mechanical and tribological properties of W_2N films by doping silicon, Surf. Coat. Technol. 317 (2017) 158–165. ISSN 0257-8972.
[4] H. Ju, L. Yu, S. He, I. Asempah, J. Xu, Y. Hou, The enhancement of fracture toughness and tribological properties of the titanium nitride films by doping yttrium, Surf. Coat. Technol. 321 (2017) 57–63. ISSN 0257-8972.
[5] Y. Qiu, S. Zhang, B. Li, Y. Wang, J.-W. Lee, F. Li, D. Zhao, Improvement of tribological performance of CrN coating via multilayering with VN, Surf. Coat. Technol. 231 (2013) 357–363. ISSN 0257-8972.
[6] O. Knotek, M.B. hmer, T. Leyendecker, On structure and properties of sputtered Ti and Al based hard compound films, J. Vacuum Sci. Technol. A 4 (6) (1986) 2695–2700. ISSN 0734-2101.
[7] P. Mayrhofer, R. Rachbauer, D. Holec, F. Rovere, J. Schneider, Protective transition metal nitride coatings, 355–388, 2014.
[8] A. Kimura, H. Hasegawa, K. Yamada, T. Suzuki, Effects of Al content on hardness, lattice parameter and microstructure of $Ti_{1-x}Al_xN$ films, Surf. Coat. Technol. 120 (1999) 438–441. -121ISSN 0257-8972.
[9] U. Wahlström, L. Hultman, J. Sundgren, F. Adibi, I. Petrov, J. Greene, Crystal growth and microstructure of polycrystalline $Ti_{1-x}Al_xN$ alloy films deposited by ultra-high-vacuum dual target magnetron sputtering, Thin. Solid. Films. 235 (1) (1993) 62–70. ISSN 0040-6090.
[10] A. Sugishima, H. Kajioka, Y. Makino, Phase transition of pseudobinary Cr-Al-N films deposited by magnetron sputtering method, Surf. Coat. Technol. 97 (1) (1997) 590–594. ISSN 0257-8972.
[11] P.H. Mayrhofer, C. Mitterer, L. Hultman, H. Clemens, Microstructural design of hard coatings, Prog. Mater. Sci. 51 (8) (2006) 1032–1114. ISSN 0079-6425.
[12] J. Caicedo, G. Zambrano, W. Aperador, L. Escobar-Alarcon, E. Camps, Mechanical and electrochemical characterization of vanadium nitride (VN) thin films, Appl. Surf. Sci. 258 (1) (2011) 312–320. ISSN 0169-4332.
[13] A.K. Verma, R. Gupta, S. Prakash, A. Gloskovskii, S. Kalal, P. Tiwari, V.R. Reddy, R. Rawat, M. Gupta, Structure and superconductivity of epitaxial and polycrystalline VN thin films, ACS. Appl. Electron. Mater. 6 (7) (2024) 5029–5035. ISSN 2637-6113.
[14] H. Ohno, Toward Functional Spintronics, Science (1979) 291 (5505) (2001) 840–841. ISSN 0036-8075.
[15] F. Miyashiro, N. Iwase, A. Tsuge, F. Ueno, M. Nakahashi, T. Takahashi, High thermal conductivity aluminum nitride ceramic substrates and packages, IEEE Trans. Compon., Hybrids, Manuf. Technol. 13 (2) (1990) 313–319. ISSN 0148-6411.
[16] H. Holleck, Metastable coatings prediction of composition and structure, Surf. Coat. Technol. 36 (1) (1988) 151–159. ISSN 02578972.
[17] P.H. Mayrhofer, D. Music, J.M. Schneider, Ab initio calculated binodal and spinodal of cubic $Ti_{1-x}Al_xN$, Appl. Phys. Lett. 88 (7) (2006) 071922. ISSN 0003-6951.
[18] I. Petrov, P.B. Barna, L. Hultman, J.E. Greene, Microstructural evolution during film growth, J. Vacuum Sci. Technol. A 21 (5) (2003) S117–S128. ISSN 0734-2101.
[19] M. Liewald, S. Wagner, D. Becker, C. Ziebert, P. Pesch, S. Kolozsvari, Experimental examination of the wear behaviour of the VAlN tool coating by strip drawing process, Int. J. Adv. Manuf. Technol. 58 (2012) 1433–3015. ISSN 0268-3768.
[20] W. Grzesik, Advanced Protective Coatings for Manufacturing and Engineering, Hanser Gardner Publications, 2003. ISBN 9781569903391.
[21] H.K. Zou, L. Chen, K.K. Chang, F. Pei, Y. Du, Enhanced hardness and age-hardening of TiAlN coatings through Ru-addition, Scr. Mater. 162 (2019) 382–386. ISSN 1359-6462.
[22] G. Greczynski, S. Mraz, H. Ruess, M. Hans, J. Lu, L. Hultman, J. Schneider, Extended metastable Al solubility in cubic VAlN by metal-ion bombardment during pulsed magnetron sputtering: film stress vs subplantation, J. Appl. Phys. 122 (2) (2017). ISSN 00218979.
[23] P. Zhu, F. Ge, S. Li, Q. Xue, F. Huang, Microstructure, chemical states, and mechanical properties of magnetron co-sputtered $V_{1-x}Al_xN$ coatings, Surf. Coat. Technol. 232 (2013) 311–318.
[24] G. Greczynski, S. Mráz, M. Hans, D. Primetzhofer, J. Lu, L. Hultman, J. Schneider, Unprecedented Al supersaturation in single-phase rock salt structure VAlN films by Al+ subplantation, J. Appl. Phys. 121 (17) (2017). ISSN 0021-8979.
[25] Y. Chim, X. Ding, X. Zeng, S. Zhang, Oxidation resistance of TiN, CrN, TiAlN and CrAlN coatings deposited by lateral rotating cathode arc, Thin. Solid. Films. 517 (17) (2009) 4845–4849. ISSN 0040-60904th International Conference on Technological Advances of Thin Films and Surface Coatings.
[26] F. Rovere, D. Music, S. Ershov, M. to Baben, H.-G. Fuss, P.H. Mayrhofer, J. M. Schneider, Experimental and computational study on the phase stability of Al-containing cubic transition metal nitrides, J. Phys. D. Appl. Phys. 43 (3) (2010) 035302. ISSN 0022-3727.
[27] L.G. Parratt, Surface studies of solids by total re ection of X-rays, Phys. Rev. 95 (2) (1954) 359.
[28] P. Gupta, P. Rao, M. Swami, A. Bhakar, S. Lal, S. Garg, C. Garg, P. Gauttam, S. Kane, V. Raghuwanshi, BL-02: a versatile X-ray scattering and diffraction beamline for engineering applications at Indus-2 synchrotron source, J. Synchrotron. Radiat. 28 (4) (2021) 1193–1201. ISSN 1600-5775.
[29] D. Phase, M. Gupta, S. Potdar, L. Behera, R. Sah, A. Gupta, Development of soft X-ray polarized light beamline on Indus-2 synchrotron radiation source, in: AIP Conference Proceedings 1591, AIP, 2014, pp. 685–686. ISSN 0735412251.
[30] W.A. Caliebe, V. Murzin, A. Kalinko, M. Gorlitz, High-flux XAFS-beamline P64 at PETRA III, in: AIP Conference Proceedings 2054, AIP Publishing, 2019. ISSN 0094-243X.
[31] C. Schlueter, A. Gloskovskii, K. Ederer, I. Schostak, S. Piec, I. Sarkar, Y. Matveyev, P. Lomker, M. Sing, R. Claessen, The new dedicated HAXPES beamline P22 at PETRAIII, in: AIP conference proceedings 2054, AIP Publishing, 2019. ISSN 0094-243X.
[32] B. Ravel, M. Newville, ARTEMIS ATHENA, HEPHAESTUS: data analysis for X-ray absorption spectroscopy using IFEFFIT, J. Synchrotron. Radiat. 12 (4) (2005) 537–541. ISSN 0909-0495.
[33] D. Gall, S. Kodambaka, M. Wall, I. Petrov, J. Greene, Pathways of atomistic processes on TiN (001) and (111) surfaces during film growth: an ab initio study, J. Appl. Phys. 93 (11) (2003) 9086–9094. ISSN 0021-8979.
[34] M.-H. Tuilier, M.-J. Pac, M. Girleanu, G. Covarel, G. Arnold, P. Louis, C. Rousselot, A.M. Flank, Electronic and atomic structures of Ti1−xAlxN thin films related to their damage behavior, J. Appl. Phys. 103 (8) (2008). ISSN 0021-8979.
[35] H. Ju, P. Jia, J. Xu, L. Yu, Y. Geng, M. Liu, T. Wei, et al., The effects of adding aluminum on crystal structure, mechanical, oxidation resistance, friction and wear properties of nanocomposite vanadium nitride hard films by reactive magnetron sputtering, Mater. Chem. Phys. 215 (2018) 368–375.
[36] S. Kolozsvari, P. Pesch, C. Ziebert, M. Stueber, S. Ulrich, Deposition and characterization of hard coatings in the material system V-Al-N by reactive magnetron sputter deposition, Plasma Process. Polym. 6 (1) (2009) S146–S151. ISSN 1612-8850.
[37] S. Liu, K. Chang, D. Music, X. Chen, S. Mraz, D. Bogdanovski, M. Hans, D. Primetzhofer, J.M. Schneider, Stress-dependent prediction of metastable phase formation for magnetron sputtered $V_{1-x}Al_xN$ and $Ti_{1-x}Al_xN$ thin films, Acta Mater. 196 (2020) 313–324. ISSN 13596454.
[38] A.R. Robertson, R.D. Lozano, D.H. Alman, S. Orchard, J. Keitch, R. Connely, L. Graham, W. Acree, R. John, R. Hoban, et al., CIE recommendations on uniform

color spaces, colordi erence equations, and metric color terms, Color. Res. Appl. 2 (5–6) (1977) 3. ISSN 0361-2317.
[39] J.A. Bearden, A. Burr, *Re*-evaluation of X-ray atomic energy levels, Rev. Mod. Phys. 39 (1) (1967) 125.
[40] V. Ivashchenko, P. Turchi, V. Shevchenko, E. Olifan, First-principles study of phase stability of stoichiometric vanadium nitrides, Phys. Rev. B Condensed Matter Mater. Phys. 84 (17) (2011) 174108. ISSN 1550-235X.
[41] J. Wong, F. Lytle, R. Messmer, D. Maylotte, K-edge absorption spectra of selected vanadium compounds, Phys. Rev. B 30 (10) (1984) 5596. ISSN 2469-9969.
[42] T. Yamamoto, Assignment of pre-edge peaks in K-edge x-ray absorption spectra of 3d transition metal:electric dipole or, Quadrupole (2008).
[43] C. Sandu, R. Sanjines, M. Benkahoul, F. Medjani, F. Levy, Formation of composite ternary nitride thin films by magnetron sputtering co-deposition, Surf. Coat. Technol. 201 (7) (2006) 4083–4089. ISSN 0257-8972.
[44] M.C. Biesinger, L.W. Lau, A.R. Gerson, R.S.C. Smart, Resolving surface chemical states in XPS analysis of first row transition metals, oxides and hydroxides: *sc*, Ti, V, Cu and Zn, Appl. Surf. Sci. 257 (3) (2010) 887–898. ISSN 0169-4332.
[45] D. Gall, R. Haasch, N. Finnegan, T.-Y. Lee, C.-S. Shin, E. Sammann, J. Greene, I. Petrov, In situ X-ray photoelectron, ultraviolet photoelectron, and auger electron spectroscopy spectra from first-row transition-metal nitrides: scN, TiN, VN, and CrN, Surf. Sci. Spectra 7 (3) (2000) 167–168. ISSN 1058-5269.
[46] S. Seema, D. Kumar, U. Deshpande, M. Gupta, Synthesis of fcc-Co from isostructural Co4N, J. Appl. Phys. 130 (12) (2021). ISSN 00218979.
[47] D. Jaeger, J. Patscheider, A complete and self-consistent evaluation of XPS spectra of TiN, J. Electron. Spectros. Relat. Phenomena 185 (11) (2012) 523–534.
[48] P. Prieto, R.E. Kirby, X-ray photoelectron spectroscopy study of the difference between reactively evaporated and direct sputter-deposited TiN films and their oxidation properties, J. Vacuum Sci. Technol. A 13 (6) (1995) 2819–2826. ISSN 0734-2101.
[49] M.J. Vasile, A.B. Emerson, F.A. Baiocchi, The characterization of titanium nitride by x-ray photoelectron spectroscopy and Rutherford backscattering, J. Vacuum Sci. Technol. A 8 (1) (1990) 99–105. ISSN 0734-2101.
[50] O. Asturizaga, R. Sanjines, G. Margaritondo, F. Levy, $TiAlVN_{1-x}$thin films deposited by reactive sputtering chemical composition, Surf. Coat. Technol. 61 (1993) 30–35. ISSN 0257-8972.
[51] P. Motamedi, K. Cadien, XPS analysis of AlN thin films deposited by plasma enhanced atomic layer deposition, Appl. Surf. Sci. 315 (2014) 104–109. ISSN 0169-4332.
[52] M. Wiesing, T. de Los Arcos, G. Grundmeier, UHV AFM based colloidal probe studies of adhesive properties of VAlN hard coatings, Appl. Surf. Sci. 428 (2018) 767–774. ISSN 01694332.
[53] R. Prakash, S. Kumar, V. Kumar, R. Choudhary, D. Phase, Optical and x-ray photoelectron spectroscopy studies of α-Al_2O_3, in: AIP Conference Proceedings 1731, AIP Publishing LLC, 2016 050097. ISSN 0735413789.
[54] I. Kabir, L. Sheppard, R. Shamiri, P. Koshy, R. Liu, W. Joe, A. Le, X. Lu, W.-F. Chen, C. Sorrell, Contamination of TiO_2 thin films spin coated on borosilicate and rutile substrates, J. Mater. Sci. 55 (9) (2020) 3774–3794. ISSN 0022-2461.
[55] P. Kubelka, F. Munk, An article on optics of paint layers, Z. Tech. Phys 12 (593–601) (1931) 259–274.
[56] K. Kuriyama, Y. Takahashi, F. Sunohara, Optical band gap of Zn_3N_2 films, Phys. Rev. B 48 (4) (1993) 2781.
[57] P. Makula, M. Pacia, W. Macyk, How to correctly determine the band gap energy of modified semiconductor photocatalysts based on UV vis spectra, 2018, J. Phys. Chem. Lett. 9 (23) (2018) 6814–6817. ISSN 1948-7185.
[58] W. Yim, E. Stofko, P. Zanzucchi, J. Pankove, M. Ettenberg, S. Gilbert, Epitaxially grown AlN and its optical band gap, J. Appl. Phys. 44 (1) (1973) 292–296. ISSN 0021-8979.
[59] R. Jalali, M. Parhizkar, H. Bidadi, H. Naghshara, S.R. Hosseini, M. Jafari, The effect of Al content, substrate temperature and nitrogen ow rate on optical band gap and optical features of nanostructured TiAlN thin films prepared by reactive magnetron sputtering, Appl. Phys. A 122 (2016) 1–7. ISSN 0947-8396.
[60] H. Buckle, J. Westbrook, H. Conrad. The Science of Hardness Testing and Its Research Applications, American Society for Metals, Materials Park, Ohio, 1971.
[61] K. Kumar, H. Van Swygenhoven, S. Suresh, Mechanical behavior of nanocrystalline metals and alloys, Acta Mater. 51 (19) (2003) 5743–5774. ISSN 1359-6454.
[62] V. Raghavan, Physical metallurgy: Principles and Practice, PHI Learning Pvt. Ltd., 2015. ISBN 97881-203-3012-2.
[63] C. Anthony, Fischer-Cripps, Nanoindentation, Springer, New York, 2011.
[64] J.J. Gilman, Chemistry and Physics of Mechanical Hardness, John Wiley & Sons, 2009. ISBN 978-0470-22652-0.